CloudSat Project

A NASA Earth System Science Pathfinder Mission

Level 2B CWC-RVOD Product

Process Description and Interface Control Document

Product version P1_R05

Document revision: 0

Date: March 7, 2019

Address questions concerning the document to:
Jussi Leinonen
Jussi.S.Leinonen@jpl.nasa.gov
+1-818-354-2788

Revision history

This is the first published revision of this document.

Changes since version R04

The release 05 algorithm is a major departure from prior version of the algorithm, which was found to have significant biases. The new algorithm is formulated using a better constrained retrieval algorithm that includes fewer free variables, and is formulated in logarithmic space. It also includes improvements to the treatment of precipitating clouds, ice clouds, and mixed-phase clouds, and uses MODIS cloud optical depth directly rather than through the CloudSat 2B-TAU product. Since MODIS cloud optical depth is only available at daytime, 2B-CWC-RVOD is now a daytime-only product.

Contents

1 Introduction

This document provides an overview of the release 05 level 2B CWC-RVOD algorithm for CloudSat. The objective of the algorithm is to determine cloud water content, with focus on liquid water, from CloudSat radar reflectivity and Aqua Moderate Resolution Imaging Spectroradiometer (MODIS) cloud optical depth. Key inputs to the algorithm are the CloudSat 2B-GEOPROF radar reflectivity [*Marchand et al.*, 2008] and the cloud optical depth variable from the collection 6 level 2 Aqua MODIS cloud product (MYD06) [*Platnick et al.*, 2003], which has been collocated to CloudSat coordinates and is available via the CloudSat MOD06-1KM-AUX product. The algorithm further makes use of ice cloud optical extinction properties given in the 2C-ICE product [*Deng et al.*, 2013, 2015], and ancillary temperature estimates from the European Centre for Medium-Range Weather Forecasts (ECMWF) analysis provided in the ECMWF-AUX product. The remainder of this document describes the algorithm in greater detail. Section 2 describes the physical basis and assumptions upon which the algorithm is based, Sect. 3 describes the algorithm output, Sect. 4 describes the known limitations, and Sect. 5 shows an example liquid water retrieval.

2 Algorithm description

A preliminary version of the algorithm has been outlined in *Leinonen et al.* [2016]. The version presented here has been extended in order to better handle complicating factors such as precipitation, overlying ice clouds, and mixed-phase clouds.

2.1 Retrieval Framework

The algorithm retrieves the microphysical values for one CloudSat column at a time. It follows an optimal estimation framework that seeks to minimize a cost function of the form

$$\Phi = [\mathbf{y} - \mathbf{F}(\mathbf{x})]^T \mathbf{S}_\mathbf{y} [\mathbf{y} - \mathbf{F}(\mathbf{x})] + [\mathbf{x} - \mathbf{x}_\mathbf{a}]^T \mathbf{S}_\mathbf{a} [\mathbf{x} - \mathbf{x}_\mathbf{a}] \tag{1}$$

where $\mathbf{y}$ represents the measurement vector, $\mathbf{x}$ is the state vector, $\mathbf{x}_\mathbf{a}$ represents *a priori* estimate of the state, $\mathbf{S}_\mathbf{y}$ is the observation error covariance matrix, $\mathbf{S}_\mathbf{a}$ is the *a priori* error covariance matrix, and $\mathbf{F}$ is the forward model that produces the measurement vector from the state vector. The error variances and covariances determine the relative influence of the terms in determining the retrieved state. The cost function is minimized using a Gauss-Newton iteration according to the optimal estimation framework [*Rodgers*, 2000], complemented with a bounded line search algorithm used to ensure convergence. The iteration finds a solution that provides an optimal match to both the observations and a priori constraints given their relative error bounds.

2.2 Measurement vector

The measurement vector $\mathbf{y}$ contains the information given by the measurements. In this algorithm,

$$\mathbf{y} = \begin{bmatrix} \ln \tau_{\mathrm{liq}} & Z_{\mathrm{dB},1} & \cdots & Z_{\mathrm{dB},n} \end{bmatrix}^T \tag{2}$$

where τ_{liq} is the optical depth from liquid and mixed-phase bins, $Z_{\mathrm{dB},i}$ is the reflectivity (dBZ units) in the ith radar bin with valid measurements, and n is the total number of bins with valid measurements. We include liquid, ice and mixed-phase bins in the state vector. The logarithm of τ is used because it allows a more linear forward model; see *Leinonen et al.* [2016] for details.

2.3 State vector

The state vector $\mathbf{x}$ contains the cloud and precipitation microphysical variables retrieved by the algorithm. For liquid water, the retrieved variables are logarithmic values of parameters of the lognormal drop size distribution (PSD). For ice, we instead retrieve the logarithm of the ice water content l_{ice}. The resulting state vector is then

$$\mathbf{y} = \begin{bmatrix} \ln N_{T,0} & \ln r_{\mathrm{g},1} & \cdots & \ln r_{\mathrm{g},n_{\mathrm{liq}}} & \ln l_{\mathrm{ice},1} & \cdots & \ln l_{\mathrm{ice},n_{\mathrm{ice}}} \end{bmatrix}^T. \tag{3}$$

where $N_{T,0}$ is the total droplet number concentration of liquid water (in non-precipitating conditions; see Sect. 2.5), r_g is the geometric mean radius for liquid water, and n_{liq} is the number of valid liquid-water and mixed-phase bins, and n_{ice} is the number of valid ice bins. The following sections describe the liquid water and ice models in more detail.

2.4 Preprocessing

Before running the optimal estimation, the column is partitioned into liquid, ice and mixed-phase parts based on the ECMWF analysis temperature. Radar bins colder than $-30^{\circ}\mathrm{C}$ are assumed to be ice-only, bins warmer than $0^{\circ}\mathrm{C}$ are considered liquid-only, and those in between are assigned as mixed-phase bins.

The total optical depth is a sum of the liquid and ice contributions:

$$\tau = \tau_{\mathrm{liq}} + \tau_{\mathrm{ice}}, \tag{4}$$

where τ_{liq} is the contribution from liquid and mixed-phase bins, and τ_{ice} is the contribution from ice bins. A good estimate of τ_{ice} can be obtained from 2C-ICE, as that product uses the CALIPSO lidar in addition to the CloudSat radar. Therefore, we subtract the 2C-ICE-derived ice optical depth τ_{ice} from the τ from Aqua MODIS to estimate τ_{liq}.

2.5 Liquid water model

The basis of the liquid water model is the lognormal size distribution

$$N(r) = \frac{N_T}{\sqrt{2\pi}\sigma_{\log} r} \exp\left(\frac{-\ln^2(r/r_g)}{2\sigma_{\log}^2}\right), \tag{5}$$

where r is the drop radius and $\sigma_{\log}$ is the scale parameter

Considering the limited number of measurements available, some simplifications have been made to the variables considered in the liquid water model: As shown in Eq. (3), we assume a constant value of N_T for the entire column (but this is adjusted in mixed-phase clouds; see Sect. 2.7. The scale parameter $\sigma_{\log}$ is fixed as at 0.38 based on *Miles et al.* [2000]. The number concentration is reduced for large drops to reflect the depletion of drops due to coalescence. The model we developed for this purpose is:

$$\ln N_T = \begin{cases} \ln N_{T,0} & r_g < r_0 \\ \ln N_{T,0} + (a \ln^2 r_g + b \ln r_g + c) & r_0 \le r_g < r_1 \\ \ln N_{T,0} + (d - 3 \ln r_g) & r_1 \le r_g. \end{cases} \tag{6}$$

The threshold radii r_0 and r_1 were found by tuning the path-integrated attenuation (PIA) produced by the model against that from surface-reference measurements; see *Lebsock et al.* [2011]; *Leinonen et al.* [2016] for the details. We obtained $r_0 = 10$ μm and $r_1 = 3000$ μm using this approach. The parameters a, b, c, d can be obtained by requiring continuity and differentiability of Eq. 6. The adjustment is negligible in most non-precipitating cases and mainly serves to produce a better estimate of moderate to heavy precipitating water content.

Since the number of state variables is equal to the number of measurements, the prior distributions can be rather loose, as the measurements constrain the state vector quite effectively. We impose a negative correlation between $\ln N_T$ and $\ln r_g$, and a distance-dependent positive correlation between $\ln r_g$ in different bins of the same column. The mean vector $\mathbf{x_a}$ and the covariance matrix $\mathbf{S_a}$ are built assuming that:

$$\mathrm{E}[\ln N_{T,0}] = 16.71 \tag{7}$$
$$\mathrm{Std}[\ln N_{T,0}] = 1.448 \tag{8}$$
$$\mathrm{E}[\ln r_g] = -11.67 \tag{9}$$
$$\mathrm{Std}[\ln r_g] = 1.497 \tag{10}$$
$$\mathrm{Cor}[\ln N_{T,0}, \ln r_g] = -0.5 \tag{11}$$
$$\mathrm{Cor}[\ln r_{g,i}, \ln r_{g,j}] = 0.3 \exp\left(-\frac{d(i,j)}{1.5}\right) + 0.7 \exp\left(-\frac{d(i,j)}{300}\right) \tag{12}$$

where $d(i,j)$ indicates the distance, in units of CloudSat bins (each 240 m high), between the ith and jth bins. The prior distribution for the liquid water is based partially on measurements

using idealized cases for nonprecipitating clouds described in *Leinonen et al.* [2016]. These have been adjusted to ensure that the resulting covariance matrix is valid (i.e. positive definite) and to allow the microphysical values to also cover precipitating conditions. In practice, it was found that retrieval is not particularly sensitive to the exact value of the priors as long as reasonable expected values and standard deviations are used.

2.6 Ice model

For ice, the retrieval is based only on the radar reflectivity. The ice retrieval is run primarily for the sake of completeness; for cloud ice water content, we recommend data users use the 2C-ICE product. The ice water product is tuned such that it is consistent with the 2C-ICE product. Like that product, 2B-CWC-RVOD uses a gamma size distribution

$$N(D) = N_0 D^{\mu} \exp(-\Lambda D) \tag{13}$$

where D is the ice particle diameter, μ is the shape parameter and Λ is the scale parameter. As with 2C-ICE, the shape is fixed at $\mu = 1$. To determine the other free parameters, we use the temperature-dependent parameterization for ice crystal number concentration by *Heymsfield et al.* [2013], modified by the total ice water content. The resulting formula is:

$$N_{T,\mathrm{ice}}(T) = \begin{cases} 27.0 \times 10^3 \ \mathrm{m}^{-3} \ C(l_{\mathrm{ice}}), & T < 45.6^{\circ}\mathrm{C} \\ 3.304 \times 10^3 \exp(-0.04607\, T) \ C(l_{\mathrm{ice}}), & \text{otherwise} \end{cases} \tag{14}$$

where the temperature is in degrees Celsius. The temperature limit between constant and variable number concentration has been adjusted from *Heymsfield et al.* [2013] in order to ensure a continuous relation. The adjustment dependent on l_{ice} was empirically determined as

$$C(l_{\mathrm{ice}}) = 0.50 \times (\ln l_{\mathrm{ice}} + 12.0) \tag{15}$$

by requiring that retrieved l_{ice} matches that from 2C-ICE on average.

2.7 Mixed-phase model

Bins with $-30^{\circ}\mathrm{C} < T < 0^{\circ}\mathrm{C}$ are considered mixed-phase. For these, the total water content is partitioned into liquid and ice components a linear transition from ice (at $-30^{\circ}\mathrm{C}$) to liquid (at $-0^{\circ}\mathrm{C}$). For mixed-phase bins, the retrieved variables are still the parameters of the liquid drop size distribution. However, a contribution from ice is added to the reflectivity, attenuation and optical depth, according to the mixing ratio and the ice model of Sect. 2.6. Since the presence of ice particles can be expected to deplete the liquid droplet number concentration, it is adjusted in mixed-phase bins by multiplying it by the liquid water fraction.

2.8 Forward model

2.8.1 Radar reflectivity

The radar reflectivity before attenuation effects is calculated as

$$Z = \frac{\lambda^4}{\pi^5 |K_w|^2} \int_0^\infty \sigma_{\mathrm{bsc}}(D) N(D)\, \mathrm{d}D \tag{16}$$

where λ is the wavelength of the radar, σ_{bsc} is the backscattering cross section, and the water dielectric factor $|K_w|^2 = 0.75$ for CloudSat [*Tanelli et al.*, 2008]. Attenuation by cloud water can be significant at the W band. For a nadir-pointing radar, the attenuated reflectivity is

$$Z'(z) = Z(z) \exp\left(-2 \int_z^{z_{\mathrm{top}}} \sigma_{\mathrm{ext}}(z')\, \mathrm{d}z' \right) \tag{17}$$

where σ_{ext} is the extinction cross section (which includes extinction due to hydrometeors and atmospheric gases), z is the altitude and z_{top} is the altitude of the top of the column. The logarithmic reflectivity, expressed in units of dBZ, as

$$Z_{\mathrm{dB}} = 10\, \log_{10} \frac{Z'}{Z_0}, \tag{18}$$

where $Z_0 = 1\ \mathrm{mm}^6\, \mathrm{m}^{-3}$. The cross sections σ_{bsc} and σ_{ext} are calculated using Mie scattering for liquid water drops. For ice crystals, they are derived from the results of *Hong* [2007a,b] for hexagonal columns, as with 2C-ICE. Z_{dB} is then derived by numerically integrating Eqs. 16 over the size distribution and 17 over the vertical column.

The error covariance matrix for Z_{dB} is assumed to be diagonal with reflectivity variance

$$\delta^2_{Z_{\mathrm{dB}}} = \delta^2_{Z_{\mathrm{dB}},\mathrm{inst}} + \delta^2_{Z_{\mathrm{dB}},\mathrm{fm}}. \tag{19}$$

where the error due to instrument noise is

$$\delta_{Z_{\mathrm{dB}},\mathrm{inst}} = \min\left[\exp\left(-0.252\, (Z_{\mathrm{dB}} + 25.0) \right) + 0.16, 1 \right] \tag{20}$$

and the error due to forward model inaccuracy (i.e. deviations from the microphysical assumptions) was estimated by *Leinonen et al.* [2016] as $3.05\ \mathrm{dB}$.

2.8.2 Cloud optical depth

The optical depth for cloud and precipitation-sized particles can be estimated at the large-wavelength limit. It is given by

$$\tau = \int_{z_{\mathrm{base}}}^{z_{\mathrm{top}}} \sigma_{\mathrm{ext,opt}}(z)\, \mathrm{d}z \tag{21}$$

$$\sigma_{\mathrm{ext,opt}} = 2A(r) N(r, z) \mathrm{d}r \tag{22}$$

where $\sigma_{\mathrm{ext,opt}}$ is the optical depth, and A is the cross-sectional area of the particle. For water droplets, this is simply

$$A(r) = \pi r^2, \tag{23}$$

while for ice crystals we use a parameterization based on the hexagonal columns of *Hong* [2007a].

The error covariance matrix for the Aqua MODIS optical depth is assumed diagonal. The error estimates from the MODIS optical depth product are used as described in *Leinonen et al.* [2016].

2.9 Data product generation

Once the microphysical variables of the liquid water drop size distribution have been retrieved, the total liquid water content can be calculated as

$$l_{\mathrm{liq}} = \int_0^\infty \frac{4\pi}{3}\rho_w r^3 N(r)\,\mathrm{d}r = \frac{4\pi}{3} N_T \rho_{\mathrm{w}} r_g^3 \exp\left(\frac{9}{2}\sigma_{\log}^2\right) \tag{24}$$

where ρ_{w} is the density of water. We also partition the water content into cloud and precipitating water by drop size. The cloud and precipitating liquid water contents can be derived from the integrals

$$l_{\mathrm{liq,cloud}} = \int_0^{r_{\mathrm{tresh}}} \frac{4\pi}{3}\rho_w r^3 N(r)\,\mathrm{d}r \tag{25}$$

$$l_{\mathrm{liq,precip}} = \int_{r_{\mathrm{tresh}}}^\infty \frac{4\pi}{3}\rho_w r^3 N(r)\,\mathrm{d}r. \tag{26}$$

The threshold used in this product is $r_{\mathrm{tresh}} = 25\ \mu\mathrm{m}$.

Liquid and ice water paths are derived by integrating the respective water contents over the vertical column:

$$L = \int_{z_{\mathrm{base}}}^{z_{\mathrm{top}}} l(z)\,\mathrm{d}z. \tag{27}$$

3 Product description

The output variables are stored in an HDF-EOS2 (HDF4) formatted file following the CloudSat conventions. Table 1 describes the variables in the output file.

Table 1: Output variables in the 2B-CWC-RVOD product.

Variable name	Unit	Data type	Dimensions	Description
Liq_Water_Content	$\mathrm{kg\,m^{-3}}$	32-bit FP	$N_{\mathrm{bin}} \times N_{\mathrm{ray}}$	Total liquid water content
Liq_Water_Content_Uncert	$\mathrm{kg\,m^{-3}}$	32-bit FP	$N_{\mathrm{bin}} \times N_{\mathrm{ray}}$	Uncertainty of the total liquid water content
Cloud_Liq_Water_Content	$\mathrm{kg\,m^{-3}}$	32-bit FP	$N_{\mathrm{bin}} \times N_{\mathrm{ray}}$	Cloud liquid water content (see Sect. 2.9 for details)
Precip_Liq_Water_Content	$\mathrm{kg\,m^{-3}}$	32-bit FP	$N_{\mathrm{bin}} \times N_{\mathrm{ray}}$	Precipitating liquid water content (see Sect. 2.9 for details)
Liq_Geom_Mean_Radius	m	32-bit FP	$N_{\mathrm{bin}} \times N_{\mathrm{ray}}$	Geometric mean radius $\exp\left(\overline{\ln r}\right)$ of liquid water drops
Liq_Geom_Mean_Radius_Uncert	m	32-bit FP	$N_{\mathrm{bin}} \times N_{\mathrm{ray}}$	Uncertainty of the geometric mean radius of liquid water drops
Liq_Number_Concentration	$\mathrm{m^{-3}}$	32-bit FP	$N_{\mathrm{bin}} \times N_{\mathrm{ray}}$	Number concentration of liquid water drops
Liq_Number_Concentration_Uncert	$\mathrm{m^{-3}}$	32-bit FP	$N_{\mathrm{bin}} \times N_{\mathrm{ray}}$	Uncertainty of the number concentration of liquid water drops
Liq_Water_Path	$\mathrm{kg\,m^{-2}}$	32-bit FP	N_{ray}	Total liquid water path
Liq_Water_Path_Uncert	$\mathrm{kg\,m^{-2}}$	32-bit FP	N_{ray}	Uncertainty of the total liquid water path
Cloud_Liq_Water_Path	$\mathrm{kg\,m^{-2}}$	32-bit FP	N_{ray}	Cloud liquid water path
Precip_Liq_Water_Path	$\mathrm{kg\,m^{-2}}$	32-bit FP	N_{ray}	Precipitating liquid water path
Ice_Water_Content	$\mathrm{kg\,m^{-3}}$	32-bit FP	$N_{\mathrm{bin}} \times N_{\mathrm{ray}}$	Ice water content
Ice_Water_Content_Uncert	$\mathrm{kg\,m^{-3}}$	32-bit FP	$N_{\mathrm{bin}} \times N_{\mathrm{ray}}$	Uncertainty of the ice water content
Ice_Water_Path	$\mathrm{kg\,m^{-2}}$	32-bit FP	N_{ray}	Ice water path
Ice_Water_Path_Uncert	$\mathrm{kg\,m^{-2}}$	32-bit FP	$N_{\mathrm{bin}} \times N_{\mathrm{ray}}$	Ice water path uncert
Phase		8-bit signed int	$N_{\mathrm{bin}} \times N_{\mathrm{ray}}$	Cloud phase: 0=missing (e.g. inside terrain), 1=ice, 2=mixed, 3=liquid
Error_Flag		16-bit signed int	N_{ray}	Error flag (see Sect. 4)
Warning_Flag		16-bit signed int	N_{ray}	Warning flag (see Sect. 4)
Radar_Reflectivity_Fwd	dBZ	32-bit FP	$N_{\mathrm{bin}} \times N_{\mathrm{ray}}$	Estimate of radar reflectivity from the forward model
PIA_Fwd	dB	32-bit FP	N_{ray}	Estimate of path integrated attenuation from the forward model

4 Known limitations

The 2B-CWC-RVOD algorithm requires that all input data be available. Thus, data availability is subject to the following limitations:

- For any periods where the 2B-GEOPROF product is not available, 2B-CWC-RVOD cannot be produced.
- MODIS cloud optical depth is based on sunlight scattered from the clouds; this limits the 2B-CWC-RVOD product to daytime-only observations.

- For certain periods of its operational history, CloudSat has not been in the A-Train constellation. There are no collocated MODIS or CALIPSO data for those periods and consequently, the 2B-CWC-RVOD data are not available. These include the period from 1 Nov 2011 (day 305) to 15 May 2012 (day 136), and the period after 22 Feb 2018 (day 53).

In case entire input data files are missing, the 2B-CWC-RVOD data files will not be produced, either. If all input files are available, the output file is produced, and the error conditions for each column are given in the Error_Flag data field. This field is set to 0 for columns that were retrieved successfully. Otherwise, the errors that apply to the column are encoded as a bit mask. Each error condition can be tested by taking the bitwise AND operation of the Error_Flag field and the applicable error. For example, a nonzero value of 'Error_Flag AND 8" indicates that the lack of optical depth prevented the running of the algorithm (most commonly, this is because the observed point was not in daylight). Table 2 lists the error codes used in this field. If the Error_Flag is set to a nonzero value, the retrieval was not run for that column.

Table 2: Error codes in the Error_Flag bit mask.

Code	Value	Description
ERR_NONE	0	No error
ERR_NO_CLOUD	1	CloudSat detected no cloud
ERR_PHASE	2	Error in phase detection prevented retrieval
ERR_PRECIP	4	Precipitation in the column is too heavy (max. radar reflectivity $Z_{\mathrm{dB}} > 20$ dBZ)
ERR_MISSING_TAU	8	Optical depth is missing
ERR_NOT_RETRIEVED	16	Retrieval was not run for other reasons
ERR_CONVERGENCE	32	Optimal estimation failed to converge

Besides the above limitations, 2B-CWC-RVOD produces an output for almost any valid input. However, some columns involved more additional assumptions than others. In order to assist users in evaluating the quality of the data, we provide the Warning_Flag field, which contains information about the additional assumptions and corrections made in order to run the retrieval. This is a bit mask of the same format as the Error_Flag field. The applicable flags are given in Table 3. Note that multiple warnings may be flagged for a single column. This simply means that all of the flagged warnings apply there independently.

Users should be particularly cautious with columns that are flagged as containing mixed-phase bins (the WRN_MIXED_PHASE flag). The algorithm employs a simple linear model of transition from liquid water to ice. While this model is consistent with climatological data, there is substantial variation around it, and thus retrievals from individual mixed-phase columns may contain significant errors. The uncertainty estimates for the liquid and ice water contents may not capture all of this uncertainty. This flag pertains to the entire column; users may find it useful to filter for liquid-only bins underneath a mixed-phase layer by testing for a zero ice water content. However, it should be noted that the mixed-phase layer still contributes to the total optical depth and to the radar attenuation, and thus errors may propagate from the mixed-phase layer to the liquid-only part of the column.

Table 3: Warning codes in the Warning_Flag bit mask.

Code	Value	Description
WRN_NONE	0	No warning (ideal liquid-water-only conditions)
WRN_ZENITH_ANGLE	1	High solar zenith angle ($> 45°$) may cause bias
WRN_ICE_CLOUD	2	Ice cloud optical depth was removed as described in Sect. 2.4
WRN_LIGHT_PRECIP	4	Light precipitation may be present (max. radar reflectivity $Z_{\mathrm{dB}} > -15$ dBZ)
WRN_MODERATE_PRECIP	8	Moderate precipitation is present (max. radar reflectivity $Z_{\mathrm{dB}} > 0$ dBZ)
WRN_MIXED_PHASE	16	Mixed-phase clouds are present in the column

Other warning flags refer to the presence of ice clouds and precipitation. The optical depth correction due to ice clouds is usually small, and thus is not expected to be a large source of error in most cases. The retrieval has also been tuned to give a reasonable result even in the presence of precipitation. Finally, a modest bias may be introduced at high solar zenith angles of the MODIS instrument, as described by *Leinonen et al.* [2016].

The Warning_Flag field can be used to identify columns where the retrieval is likely to be of high quality. On the other hand, filtering the data too aggressively may lead to sampling bias in climatological studies. Users are advised to consider the influence of such filtering on their studies on a case-by-case basis.

As mentioned earlier, the 2B-CWC-RVOD data product is focused on cloud liquid water. For cloud ice water content, we recommend that users refer to the 2C-ICE product instead.

5 Example retrieval

Fig. 1 shows an example retrieval from the algorithm.

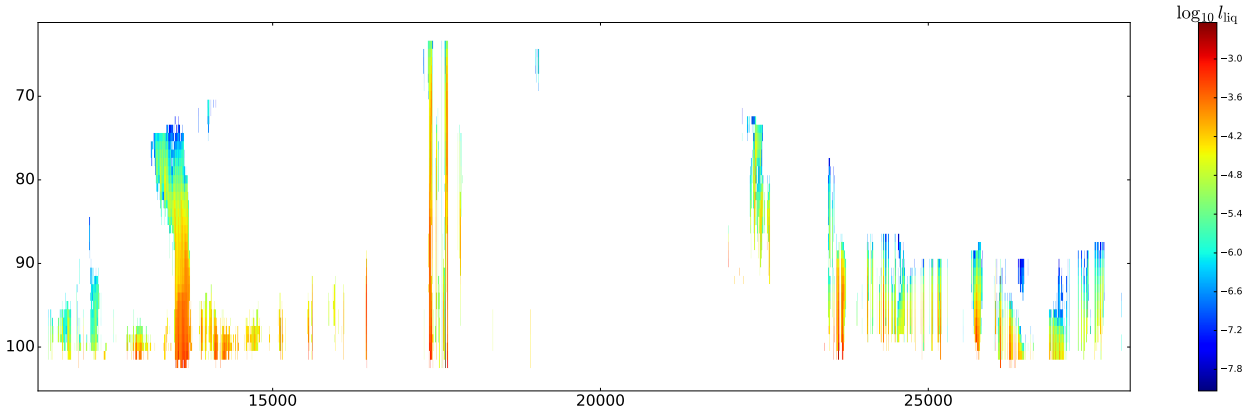

Figure 1: Example retrieval of total water content l_{liq} from a CloudSat granule. The color shows the logarithmic value $\log_{10}\, l_{\mathrm{liq}}$. The vertical and horizontal coordinates are CloudSat bin numbers.

References

Deng, M., G. G. Mace, Z. Wang, and R. P. Lawson (2013), Evaluation of several A-Train ice cloud retrieval products with in situ measurements collected during the SPARTICUS campaign, *J. Appl. Meteor. Climatol.*, *52*(4), 1014–1030, doi:10.1175/JAMC-D-12-054.1.

Deng, M., G. G. Mace, Z. Wang, and E. Berry (2015), Cloudsat 2C-ICE product update with a new Z_e parameterization in lidar-only region, *J. Geophys. Res. Atmos.*, *120*(23), 12,198–12,208, doi:10.1002/2015JD023600.

Heymsfield, A. J., C. Schmitt, and A. Bansemer (2013), Ice cloud particle size distributions and pressure-dependent terminal velocities from in situ observations at temperatures from 0° to -86°C, *J. Atmos. Sci.*, *70*(12), 4123–4154, doi:10.1175/JAS-D-12-0124.1.

Hong, G. (2007a), Parameterization of scattering and absorption properties of nonspherical ice crystals at microwave frequencies, *J. Geophys. Res.*, D11208, doi:10.1029/2006JD008364.

Hong, G. (2007b), Radar backscattering properties of nonspherical ice crystals at 94 GHz, *J. Geophys. Res.*, D22203, doi:10.1029/2007JD008839.

Lebsock, M. D., T. S. L'Ecuyer, and G. L. Stephens (2011), Detecting the ratio of rain and cloud water in low-latitude shallow marine clouds, *J. Appl. Meteor. Climatol.*, *50*(2), 419–432, doi:10.1175/2010JAMC2494.1.

Leinonen, J., M. D. Lebsock, G. L. Stephens, and K. Suzuki (2016), Improved retrieval of cloud liquid water from CloudSat and MODIS, *J. Appl. Meteor. Climatol.*, *55*(8), 1831–1844, doi:10.1175/JAMC-D-16-0077.1.

Marchand, R., G. G. Mace, T. Ackerman, and G. Stephens (2008), Hydrometeor detection using *Cloudsat* — an Earth-orbiting 94-GHz cloud radar, *J. Atmos. Oceanic Technol.*, *25*, 519–533, doi:10.1175/2007JTECHA1006.1.

Miles, N. L., J. Verlinde, and E. E. Clothiaux (2000), Cloud droplet size distributions in low-level stratiform clouds, *J. Atmos. Sci.*, *57*(2), 295–311, doi:10.1175/1520-0469(2000)057¡0295:CDSDIL¿2.0.CO;2.

Platnick, S., M. King, S. Ackerman, W. Menzel, B. Baum, J. Riedi, and R. Frey (2003), The MODIS cloud products: algorithms and examples from Terra, *IEEE Trans. Geosci. Remote Sens.*, *41*(2), 459–473, doi:10.1109/TGRS.2002.808301.

Rodgers, C. D. (2000), *Inverse Methods for Atmospheric Sounding — Theory and Practice*, World Scientific Publishing, Singapore, doi:10.1142/9789812813718.

Tanelli, S., S. L. Durden, E. Im, K. S. Pak, D. G. Reinke, P. Partain, J. M. Haynes, and R. T. Marchand (2008), CloudSat's cloud profiling radar after two years in orbit: Performance, calibration, and processing, *IEEE Trans. Geosci. Remote Sens.*, *46*(11), 3560–3573, doi:10.1109/TGRS.2008.2002030.